Andean Geology 49 (2): 185-207. May, 2022
doi: 10.5027/andgeoV49n2-3400

Andean Geology
www.andeangeology.cl

Characterization and distribution of adularia and other alteration minerals by X-ray diffraction analysis at the El Peñón Au-Ag epithermal deposit, northern Chile

***Jorge E. Morales-Leal[1], Andrew Menzies[1, 2], Hans-G. Wilke[3], José Zuluaga[4]**

[1] *Departamento de Ciencias Geológicas, Universidad Católica del Norte, Av. Angamos 0610, Antofagasta, Chile. jml011@alumnos.ucn.cl; andrew.menzies@bruker.com*

[2] *Bruker Nano GmbH, Am Studio 2D, 12489, Berlin, Germany.*

[3] *Servicios Geológicos y Paleontológicos ANQA, Av. General Bernardo O'Higgins 1650, d. 2005, Antofagasta, Chile. hgbw1953@gmail.com*

[4] *Compañía Minera Meridian Limitada, Avda. General Velázquez 890, Antofagasta, Chile. zuluagaji@gmail.com*

* *Corresponding author: jml011@alumnos.ucn.cl*

ABSTRACT. The El Peñón low-sulfidation epithermal deposit, located in the Paleocene metallogenic belt in the Antofagasta region, northern Chile, consists of Au-Ag bearing veins and hydrothermal breccias hosted in volcanic rocks and surrounded by alteration haloes consisting of a series of minerals, such as adularia, carbonates and clay minerals. They are the result of metasomatism generated by the passage of reduced, and near neutral pH, hydrothermal fluids, that transported gold through structures and its interaction with the host rock. We investigated the spatial distribution of these minerals (mainly adularia) in the Aleste vein and its host rock, located in the northern part of the district, to establish their relationship with the Au-Ag ore and, thus, support the identification of new exploration targets. An X-ray diffraction technique to discriminate adularia from other K-feldspars in whole rock samples was developed by the detail study of the diffractogram patterns of an adularia standard. The study of an X-ray diffraction standard pattern allowed the recognition of this mineral by 4 secondary peaks. Our results indicated that adularia occurs in association with felsic volcanic rocks, and it is restricted in intermediate composition units. The spatial distribution of this mineral is correlated with the mineralized zones, being adularia semi-quantitative abundance in the range of 25 to 40% a good indicator of gold mineralization. Sericite and illite occur mainly where adularia is scarce or absent. The spatial distribution of these minerals showed the structural control in the evolution and flow path of the hydrothermal fluids toward the surface. Kaolinite is related to argillic alteration caused by steam-heated fluids, and the advanced argillic alteration associated with later supergene alteration. Chlorite usually is far from the mineralized areas; therefore, it could be a reliable indicator of the margins of the system. The characterization and spatial distribution pattern of the alteration minerals identified by the X-ray diffraction method in the veins of El Peñón deposit show the capability of this type of analyses in determining possible prospection targets.

Keywords: El Peñón, Low sulfidation, Sulfidation, Epithermal, Adularia, Prospection, X-ray diffraction.

RESUMEN. Caracterización y distribución de adularia y otros minerales de alteración mediante análisis de difracción de rayos X en el depósito epitermal El Peñón, norte de Chile. El depósito epitermal de baja sulfuración El Peñón, ubicado en el cinturón metalogénico del Paleoceno, en la región de Antofagasta, norte de Chile, está constituido por vetas y brechas portadoras de Au-Ag hospedadas en rocas volcánicas hidrotermalmente alteradas. Las vetas y halos de roca alterada contienen minerales como adularia, carbonatos y arcillas generados por el metasomatismo producto de la interacción de la roca huésped con fluidos hidrotermales, de características reducidas, pH cercano a neutro y enriquecidos en oro que circularon por estructuras. En este trabajo se estudia la distribución espacial de estos minerales (en particular de adularia) en la veta Aleste y en su roca hospedante, localizada en la parte norte del distrito, con la finalidad de establecer su relación con la mena de Au-Ag y, así, apoyar la identificación de nuevos objetivos de exploración. Para esto se desarrolló una metodología de difracción de rayos X, en muestras de roca total, para diferenciar adularia de otros feldespatos potásicos mediante 4 picos secundarios presentes en el patrón de difracción de este mineral. Además, se realizaron perfiles de distribución de adularia y otros minerales de alteración hidrotermal en una sección transversal a la veta Aleste. Los resultados indican que la adularia se produce en asociación con rocas félsicas y está restringida en unidades de composición intermedia. Este mineral se correlaciona con las zonas mineralizadas y su abundancia semicuantitativa entre 25 a 40% de adularia es un buen indicador de mineralización. La sericita e illita se presentan principalmente donde la adularia es escasa o ausente. Estos minerales mostraron el control estructural en la evolución y trayectoria de los fluidos hidrotermales hacia la superficie. La caolinita está relacionada con la alteración argílica causada por el vapor de fluidos hidrotermales y la alteración argílica avanzada asociada a una alteración supérgena posterior. La clorita suele estar lejos de las áreas mineralizadas; por lo tanto, podría ser un indicador confiable de los márgenes del sistema. La caracterización y distribución de los minerales de alteración por el método de difracción de rayos X en las vetas del depósito El Peñón muestran la capacidad de este tipo de análisis para determinar posibles objetivos de prospección.

Palabras clave: El Peñón, Baja sulfuración, Sulfidación, Epitermal, Adularia, Prospección, Difracción de rayos X.

1. Introduction

Epithermal deposits have been widely studied by several authors (*e.g.*, Hedenquist *et al*., 2000; Simpson *et al*., 2001; Sillitoe and Hedenquist, 2003; Camprubí *et al*., 2003; Camprubí and Albinson, 2006; Holley *et al*., 2016). These deposits are formed by hydrothermal fluid at a temperature between 100 to 320 °C, commonly 1 km below the water table (Camprubí *et al*., 2003). Based on the ore mineralogy, these types of deposits are classified into three end member types: high-sulfidation (HS), intermediate-sulfidation (IS), and low-sulfidation (LS) (*e.g.*, Hedenquist *et al*., 2000; Sillitoe and Hedenquist, 2003).

Specifically, LS epithermal deposits are formed by boiling fluids that are concentrated in permeable zones of the upper earth crust, analogous to geothermal active systems (Sillitoe, 2015) which are generated during discharge of a spectrum of fluid types under varied conditions. The ore-forming solutions (near neutral pH chloride waters) are mainly compounded by meteoric water which descends to deep areas through permeable zones, leaching the host rock and enriching the fluid in elements such K^+ (Simmons *et al*., 2005; Warren *et al*., 2007) with a nil to small and variable component of magmatic water. Later on these solutions are heated, *e.g.*, by an intrusive body or volcanic complex, producing its ascent to the surface through permeable zones and structures (Hedenquist *et al*., 2000; Sillitoe and Hedenquist, 2003; Camprubí and Albinson, 2006). Subsequently, the complex ions solubility decreases as a result of the fluid rising to a shallower environment, precipitating minerals at the moment of boiling and subsequent drop in temperature, inside structures, forming veins filled by copper and silver sulfosalts, silver sulfides, halides, electrum, native gold, and silver, accompanied by hydrothermal minerals as adularia, quartz, K-bearing clays, and carbonates (Simmons *et al*., 2005). El Peñón Au-Ag deposit, located in the Paleocene metallogenic belt in the Antofagasta region, Chile (Fig. 1; Camus, 2003), is an example of a LS epithermal deposit. This deposit is characterized by gold and silver mineralization hosted in "bonanza-type" veins and hydrothermal breccias, both filled by quartz-adularia-carbonate alteration minerals (Sillitoe, 1993) that are hosted in Lower Cretaceous to Early Eocene volcanic rocks of rhyolitic to andesitic composition (Zuluaga, 2004).

The mineralizing hydrothermal fluids of LS deposits generate the alteration of the wall-rock usually by hydrolysis, hydration-dehydration, decarbonization, silicification and oxide-reduction reactions (Guilbert and Park, 2007). The intensity of this metasomatism

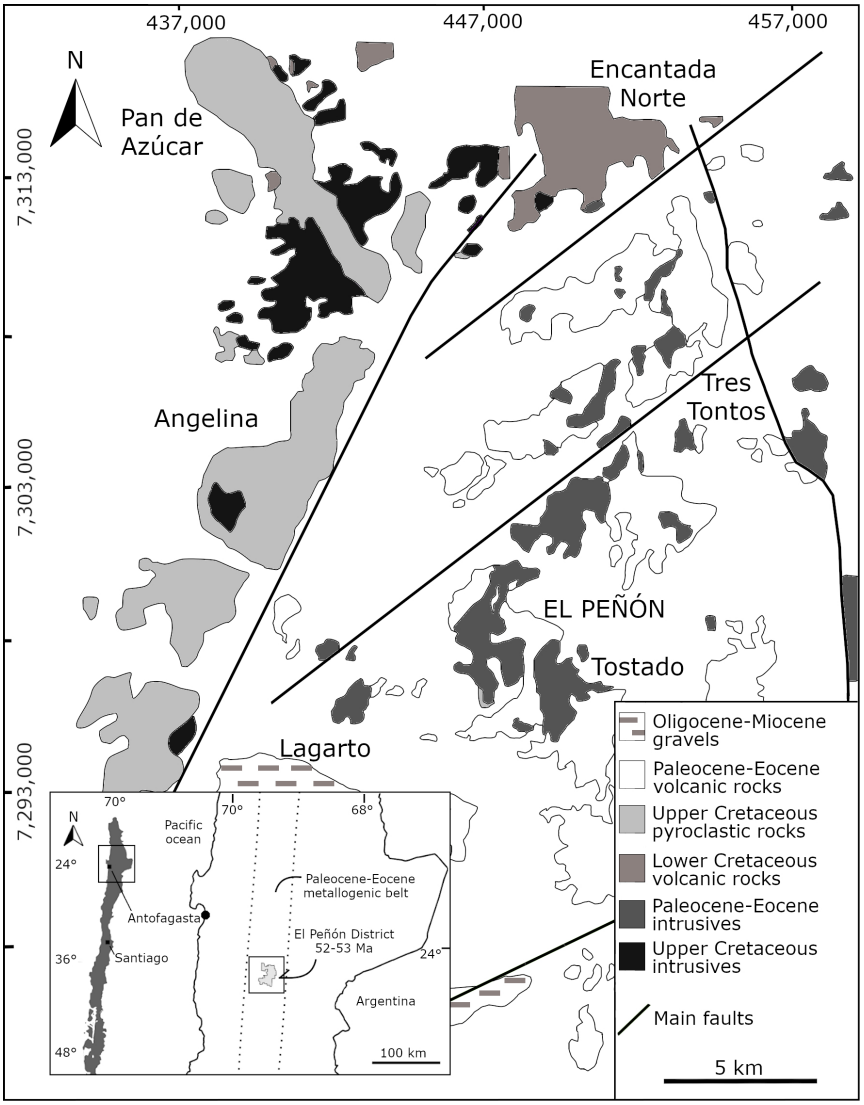

FIG. 1. Location of the El Peñón deposit and simplified geological map of the district. Modified from Zuluaga (2004) and Warren *et al*. (2007).

is a consequence of the rock reactivity and the time of contact. The thermodynamic disequilibrium, resulting from the water-rock interaction, results in the dissolution of minerals, changes to the rock texture and formation of new mineral phases which are stable in the new hydrothermal conditions (Einaudi *et al*., 2003; Hedenquist *et al*., 2000; Sillitoe and Hedenquist, 2003; Warren *et al*., 2007). According to Giggenbach (1988), near the veins, in LS systems, a potassium metasomatism accompanied by silica deposition occur due to the rise of the fluids with precipitation of adularia, quartz, and carbonates, in addition to the dissolution of minerals containing Ca, Mg and Na. In the outwards areas far from the mineralized veins (until ~50 m) a hydrogen metasomatism dominates at a condition of sub-boiling temperatures (Warren *et al*., 2007). Furthermore, in the upper part of the system, the presence of steam-heated CO_2-rich waters, and acidity raises lead to the formation of calcite and Al-bearing minerals

such as kaolinite and minor alunite. In distal areas, where the meteoric water recharges the system, a Mg- and Ca- metasomatism occurs producing the dissolution of K-bearing minerals during the heating of the infiltrated fluids, enriching the fluid in K^+, while Mg^{2+} and Ca^{2+} precipitate forming calcite and chlorite in the altered rock. Moreover, albite can be formed by minor Na metasomatism, if this mineral already exists in the wall rock, it is preserved. These reactions generate a series of alteration haloes, highlighting an assemblage quartz + calcite + adularia ± illite in the veins and near to them. This alteration is the one that contains the mineralization. Then moving away from the vein (until ~50 m), this alteration gradually changes to illite, illite-smectite layers, smectite, usually with pyrite and carbonates. Finally, a propylitic alteration that includes quartz, albite, chlorite, calcite, pyrite, and epidote dominate at distal part of the system (>50 m; Camprubí and Albinson, 2006; Hedenquist *et al*., 2000; Sillitoe and Hedenquist, 2003; Simmons *et al*., 2005; Warren *et al*., 2007).

The mineral phases that compose the alteration haloes are essential for the prospection of these types of deposits, being adularia, a potassium feldspar of low temperature, one of the minerals of most interest. Nevertheless, the recognition of this phase in hand specimens and thin sections could be difficult and problematic, especially if the adularia coexists with orthoclase, or other potassium feldspar minerals, which could be wall rock mineral components and not necessarily be part of the hydrothermal process. Therefore, the use of an analytical mineralogical method could be a feasible solution for the recognition of this mineral. Hence, the objective of this study is to develop a methodology to identify and quantify the adularia presence in the deposit by using X-ray diffraction (XRD) analysis. This will be accomplished by the detailed study of an adularia diffractogram pattern and comparing it with a series of diffractograms generated from samples collected in a cross section to the Aleste vein, one of the largest veins in the El Peñón deposit. In addition, the data will use to elaborate a cross section with the distribution of this mineral and other alteration phases around the veins of the deposit, emulating the adularia cross section recognized in the veins of Golden Cross deposit, New Zealand (Simpson *et al*., 2001). This study will provide a method for identifying adularia, and a deeper understanding of the behavior of this mineral, together with other alteration minerals, in the epithermal environment, and thus facilitate the work for geologists in the prospection of LS deposits.

2. Geological settings

The El Peñón deposit is located in the Paleocene-Eocene Metallogenic belt located to the west of Cordillera de Domeyko and in the Central depression of Chile (Fig. 1; Boric *et al*., 1990). This belt has an extension of ~1,300 km from the southern Peru to central-north of Chile (~29° S) and 30 to 50 km width, hosting several Au-Ag epithermal and porphyry copper deposits (Boric *et al*., 1990; Marinovic *et al*., 1995).

2.1. Geology of the deposit

The El Peñón deposit (Fig. 1) is formed by volcanic rocks and rhyolitic domes intruded by a series of Upper Cretaceous to Eocene intrusives (Cabello, 1999; Pérez *et al*., 1999; Cornejo *et al*., 2003; Matthews, 2009; Zuluaga, 2004; Warren *et al*., 2004, 2007). The stratified units are fundamentally volcanic rocks deposited in continental environments which include: (**i**) Lower Cretaceous andesitic-dacitic volcanic sequence; (**ii**) Upper Cretaceous pyroclastic rocks sequence; and (**iii**) Paleocene-Eocene andesitic-basaltic lavas and rhyolitic domes (Zuluaga, 2004). These sequences are intruded by Upper Cretaceous to Eocene intrusive bodies of different compositions such as dioritic-monzodioritic, andesitic-monzonitic and dacitic-rhyolitic rocks (Zuluaga, 2004).

The main structures of the district are two subparallel regional faults. The first is the Dominador Fault, with NNE direction and east dip, which delimits the Upper Cretaceous rocks with Paleocene-Eocene units to the west of the district. The second one is the NS-direction, and subvertical dip La Mula Fault that separates Paleogene rock units to the east of the district. These structures have been described as normal faults forming a graben where is the El Peñón deposit, nevertheless, transcurrent activity of these faults have been informed. The N-S structural domain is hosting Au-Ag bearing veins in its central block. To the north, the mineralized block is delimited by N40E faults (Zuluaga, 2004; Donoso, 2012).

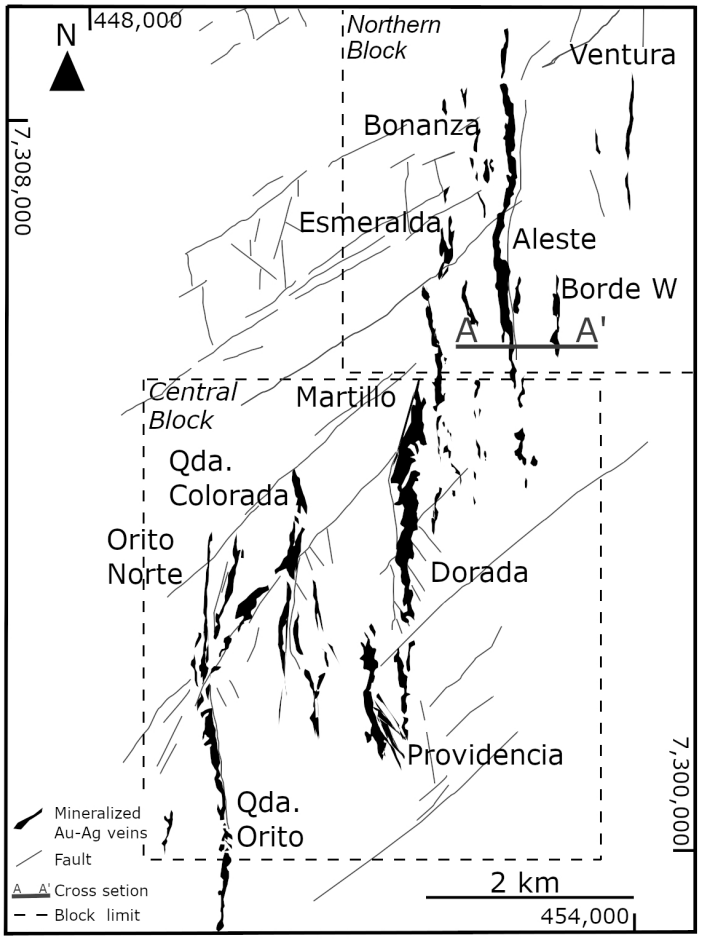

FIG. 2. Map of distribution of the main veins of the El Peñón deposit. The A-A' line over Aleste vein shows the position of the cross section studied in this work (7,305,100 m N).

2.2. Au-Ag ore and hydrothermal alteration at El Peñón

The El Peñón gold and silver ore is hosted in bonanza veins, hydrothermal breccias, and stockworks filled with quartz, adularia, and carbonates (Fig. 2). The Northern block hosts the Aleste and Bonanza veins, two of the most important veins in the district. These veins have north-south extensions of 1.5 km, and ~0.5 to 3.5 m width. Additionally, the veins tend to be wider at depth and form irregular bodies associated with intercalations of veins and hydrothermal breccias with different gold and silver grades (Donoso, 2012). In both the Central and Northern blocks (Fig. 2), the hydrothermal activity that gave rise to these veins is related to the last three pulses of five magmatic events recognized in the area. The ages of mineralization events are 52.47±0.12, 52.02±0.10 and 51.27±0.17 Ma determined by K-Ar dating (Matthews, 2009).

The gold and silver minerals are occluded or associated with base metal sulfides (Pb, Zn, Cu, Fe), Cu and Ag sulfosalts, Ag sulfides, halides, or as electrum (Donoso, 2012). The veins are made of quartz-adularia-carbonate, such as calcite, rhodochrosite, ankerite, and siderite (Zuluaga, 2004; Warren *et al*., 2008; Donoso, 2012). The upper zone of the veins is oxidized and characterized by the association of fluorite, limonite, cerussite, smithsonite, azurite, brochantite, chlorargyrite, bromargyrite, argentojarosite, native gold and silver. Below this is the mixed zone with hemimorphite,

Ag-galena, acanthite, freibergite, proustite, miargyrite, sphalerite, polybasite, electrum, bornite, chalcocite and covelline. Finally, in the deepest part is the primary sulfide zone with pyrargyrite, tetrahedrite, galena, sphalerite, chalcopyrite, pyrite, and gold (Donoso, 2012).

The hydrothermally altered wall rocks around the main veins change from intense to weak altered moving some meters away from the core of the vein. Its mineral association includes quartz, adularia, albite, illite, illite-smectite interlayered, smectite, chlorite, carbonate, and pyrite. The veins present an assemblage of crustiform and colloform banded quartz, adularia, platy calcite (lattice texture) and pseudomorphs quartz; a few meters from the core of the vein, adularia alters to illite as do the wall rocks minerals, then illite-smectite, and finally to smectite, always accompanied by quartz (quartz, calcedony and opal), and carbonate minerals. Furthermore, far from the nucleus of the veins, a weak to intense propylitic alteration characterized by chlorite, calcite, and albite assemblage can be observed, additionally, Zuluaga (2004) extend this alteration at deep (~300 m) with a propylitic association of quartz, potassium feldspar, micas, chlorite, pyrite, calcite, and minor epidote at temperatures above 250 °C. Furthermore, near the surface, and distal areas of the system, an argillic alteration characterized by an assemblage of illite, smectite, kaolinite, calcite and calcedony, derived from CO_2-enriched fluids can be observed (Zuluaga, 2004; Warren *et al*., 2007). Above the water table, acid-sulfate waters produce an alunite, kaolinite, and amorphous silica mineral assemblage. Finally, siliceous sinter was formed when the fluids reached the surface in the last state of the hydrothermal system evolution (Hedenquist *et al*., 2000; Zuluaga, 2004; Sillitoe, 2015).

3. Methodology

3.1. Sample preparation and XRD analyses

The profile selected for this study crosses the Aleste Vein and has an extension of 1.2 km (Fig. 2). The selected samples within the studied section, consist of 152 specimens, from 9 drill-cores (Fig. 3). All the samples were analyzed at the XRD/XRF laboratory at Universidad Católica del Norte. The samples were pulverized in an agate mortar and sieved through a 270 Tyler mesh (74 μm). Then, 2 g of the powder were used for the XRD analyses. The analyses were conducted in a Siemens D5000 scintillation diffractometer operating at 30 mA and 40kV, using Cu Kα1 radiation. The scan range was 3 to 70° of 2θ with a step size of 0.020° (2θ) per step time of 1 second. All the samples were measured with the same parameters in order to conserve experimental conditions. The Powder Diffraction File database (PDF-2), from the Centre for Diffraction

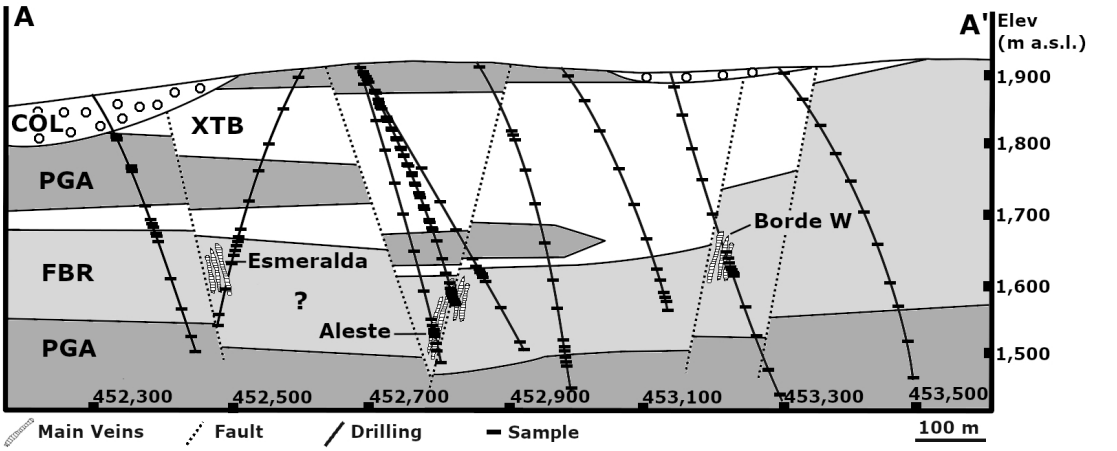

FIG. 3. Simplified geology and informal lithological units in the A-A' cross-section in figure 1. Drill holes and the location of the samples used in this study are also shown. **PGA:** andesites and dacites; **FBR:** banded fluidal rhyolite; **XTB:** litho-crystalline tuff; **COL:** coluvio.

Data (ICDD) was used for mineral identification. The semi-quantification of the multimineral diffractograms was bases in the Rietveld refinement using the Total Pattern Analysis Software (TOPAS). This software uses the crystal structures, lattice parameters and crystallographic data of each mineral for the iteration. semi-quantitative iteration parameters are shown in Supplementary material 1.

3.2. Adularia identification

An adularia crystal from Ag-Au epithermal veins from the Guanajuato Mining District, Mexico (Gross, 1975), was used as a standard to find the pattern that would permit the identification of this mineral in the studied samples diffractograms. The Guanajuato adularia was supplied by the Yamana Gold Company, no further information about it was provided. This specimen was analyzed by XRD to obtain a monomineralic diffractogram (Fig. 4A), the mineral was identified by using the *high sanidine pattern* from Bernic Lake Manitoba, Canada from the PDF-2 (code: 80-2106; Ferguson, *et al*., 1991). The mineral from which the *high sanidine pattern* was made is a mineral component of hydrothermal veins and massive quartz druses from the Buck Claim Pegmatite in the southeast of Manitoba, Canada (Lenton, 1979; Černý and Champman, 1984; Ferguson *et al*., 1991). This standard indicates a hydrothermal adularia crystal with a crystallographic structure of high sanidine content that is extremely pure (Na-poor), where Si and Al are completely disordered in their crystallographic structures. Once this standard pattern was determined, the following hypothesis was proposed, the El Peñón adularia is crystallographic and chemically the same as the Guanajuato adularia used as the standard. Consequently, both diffraction patterns are considered equal. Then, a *high sanidine pattern* was stablished to detect peaks that differentiate adularia from other potassium feldspars.

3.3. Adularia content quantification

XRD analysis provides a semi-quantitative measure of abundance of the mineral phases present

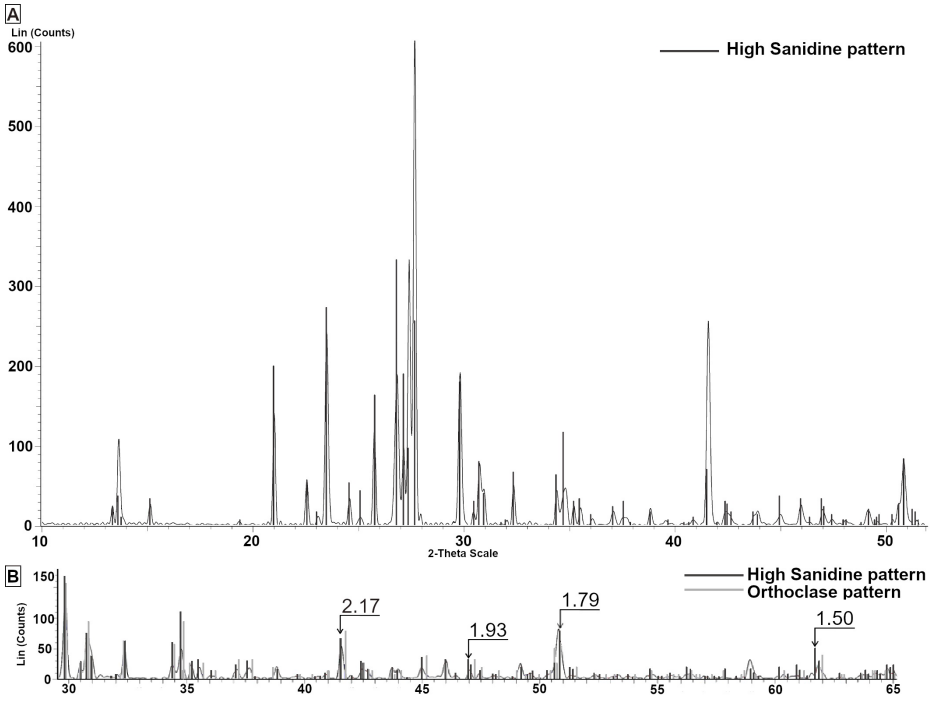

FIG. 4. **A.** Standard adularia diffractogram with the assigned high sanidine pattern. **B.** Diffractogram between 2θ=30° to 2θ=65° showing the 4 peaks, and their d-spacing (number above the peak), used to recognize adularia. The similarity between both high Sanidine and Orthoclase patterns can be observed.

in certain diffractograms. Nevertheless, when a series of quantifications of the same pattern are run by TOPAS software some similitudes in the abundance values can be observed. Therefore, in order to determine if the semi-quantification content of adularia and orthoclase are possible in the same sample, and obtaining a percentage not far from the total abundance of K-feldspar, the following three iteration models were made when adularia was detected: **1**) Semi-quantification considering orthoclase as a representative of K-feldspar groups (excluding adularia); **2**) Semi-quantification considering adularia as a representative of K-feldspar groups (excluding orthoclase); and finally, **3**) Semi-quantification considering both orthoclase and adularia.

These three iteration models determine if the similarity in adularia and orthoclase patterns generate abundance problems in the quantification of the total K-feldspar and provide abundance values of each mineral in the sample. Thus, the first two iterations must be similar in order to determine the total abundance of K-feldspar. The third iteration differentiates the percentage of abundance between both minerals. If the K-feldspar total abundance in the third iteration does not coincide with the other two, a second revision of the diffractogram is done to check for confirmation of the presence of both minerals, or to discard one of them. To see an example of this iteration method, consult Supplementary material 2.

The mineralogical profiles were created with the data from iteration (**3**), when both adularia and orthoclase were present in the diffractogram. Iteration (**1**) or (**2**) was used when only one of these mineral phases was detected. As a result, only one semi-quantification data per sample was obtained (Supplementary material 3).

4. Results

4.1. Adularia detection and semi-quantification in XRD diffractograms

The adularia and orthoclase patterns in the PDF-2 database yielded four useful secondary peaks (Table 1 and Fig. 4B) that differentiate adularia from orthoclase in the diffractograms of the studied samples. The differences of the secondary order peaks in both patterns are due to variations in the adularia crystallinity, and/or presence of trace elements in its crystallographic structure, caused by differences in the geological environments at the moment of mineral precipitation (Colville and Ribbe, 1968; Stewart and Ribbe, 1969; Ferguson *et al*., 1991).

The mineral quantifications show that adularia has a wide range of abundance. The results of the semi-quantification of this mineral together with orthoclase in the same diffractogram agree with the results of the other two quantifications mentioned in the methodology. However, some values of adularia could be slightly overestimated in some samples due to the TOPAS software uses the main peak areas in the diffractogram to calculate the relative abundance of each phase; a large part of these areas are composed of the main peaks of both minerals which are almost locate in similar positions.

4.2. Mineral distribution

4.2.1. Adularia

The distribution of adularia around the Aleste vein is shown in figure 5. This cross section shows that adularia has lithological control in its spatial distribution, predominantly related to the rhyolitic volcanic rock (FBR unit in Fig. 5), and it is restricted in the other rock units. There is a secondary structural control in its distribution associated with the veins.

TABLE 1. XRD PEAKS USED FOR ADULARIA RECOGNITION IN THIS WORK.

Secondary Peaks of adularia standard (high sanidine pattern) for adularia recognition

h	k	l	d-Spac	Intensity (Lin (count))
-2	0	4	1.79	25
0	6	0	2.17	21
2	8	0	1.50	16
-2	6	1	1.93	10

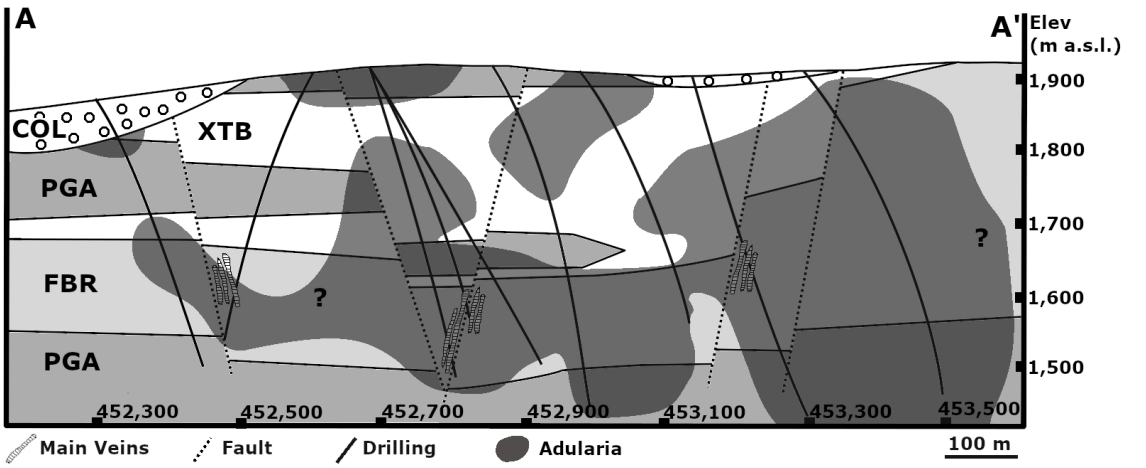

FIG. 5. Distribution of adularia in the A-A' cross section over the Aleste vein. The spatial distribution of adularia shows a strong correlation with rhyolite (FBR unit), and a secondary structural control related to veins. Lithologic units as in figure 3.

Near the surface is usually absent. Moreover, X-ray diffraction analyses indicated that adularia is associated with high contents of quartz, which is consistent with the quartz-adularia alteration within and near the veins. In addition, this mineral can be accompanied by sericite, illite, calcite, siderite, rhodochrosite, ankerite, pyrite, chlorite, and kaolinite.

The semi-quantitative contents of adularia obtained from the quantification of the diffractogram were plotted in the Aleste vein cross section (Fig. 6). This section shows a strong correlation between an adularia abundance between 25 and 40% with gold mineralized zones in the veins.

4.2.2. Sericite and illite

These two minerals represent the quartz-sericite-illite and argillic alteration zones of the ore deposits, respectively. The cross section in figure 7 shows the semi-quantitative distribution of sericite and illite, from the vein core to the outward zones. These minerals are abundant near the surface and to a depth of ~150 m, in some areas until ~250 m. The distribution of these minerals coincides with areas of low content or no adularia (Fig. 7A). In figure 7A, the sericite cross section shows this mineral above the adularia halo (quartz-adularia alteration). On the other hand, illite is distributed mostly near the surface, less than ~100 m depth (Fig. 7B). At a depth of ~80 m a transition zone between these minerals, that represent the grading from the quartz-sericite-illite to argillic alterations, is observed. The XRD analyses show that sericite is associated with quartz, illite, kaolinite, calcite, ankerite, siderite, gypsum, pyrite, chlorite, and a lesser amount of montmorillonite. Alternatively, Illite is accompanied by kaolinite, chlorite, hematite, anhydrite, calcite, siderite, ankerite and magnesite, and trace amounts of montmorillonite, jarosite, natrojarosite, pyrite and alunite.

4.2.3. Kaolinite

A kaolinite semi-quantitative distribution is shown in figure 8A. The highest values of this mineral are observed in the central east part of the cross section with semi-quantitative contents over 8%. The XRD analyses show two mineral associations that accompanied kaolinite: **i**) quartz, carbonates, montmorillonite, sericite and/or illite, and **ii**) chlorite, carbonates, gypsum, hematite, montmorillonite, heulandite, and jarosite assemblages.

4.2.4. Chlorite

This mineral represents the propylitic alteration which is present in the distal zones of the epithermal system, and areas related to andesitic dikes with a high content of Na-, Mg- and Ca-bearing minerals that induce the formation of chlorite, calcite, and epidote as alteration minerals. Chlorite distribution is shown in figure 8B. The highest values of this mineral is where adularia is scarce or absent.

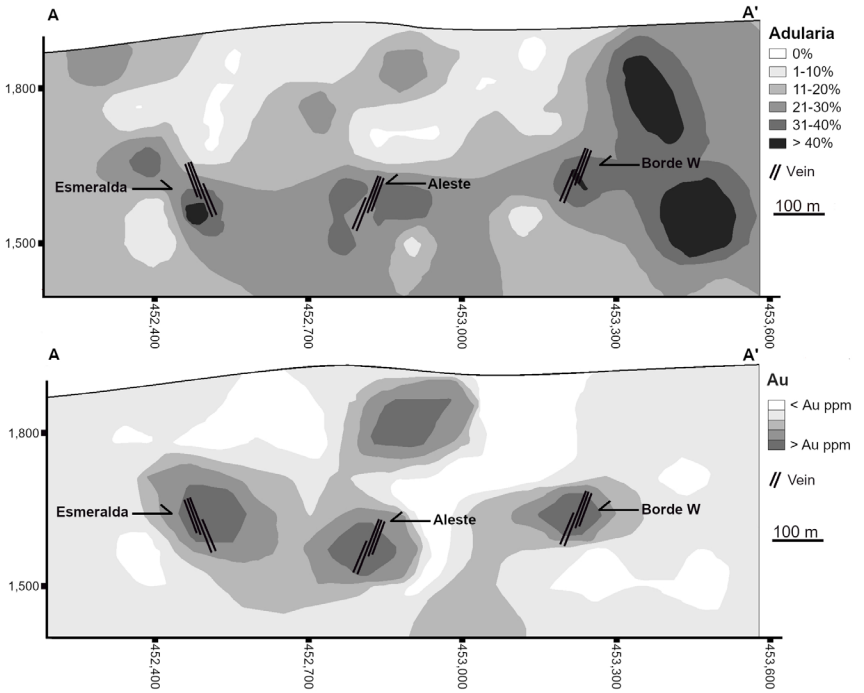

FIG. 6. Comparison between adularia distribution (above) and gold-silver veins (below) in the cross section over the Aleste vein. There is a distinct relationship between the higher adularia concentrations and the gold mineralized zones in the veins.

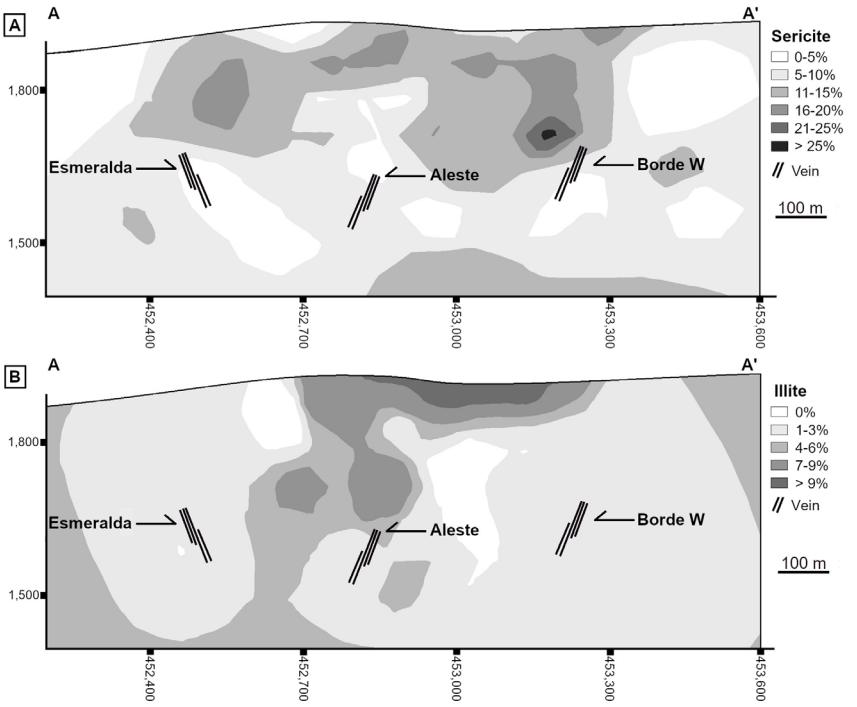

FIG. 7. Distribution of sericite (A) and illite (B) in the Aleste vein cross section.

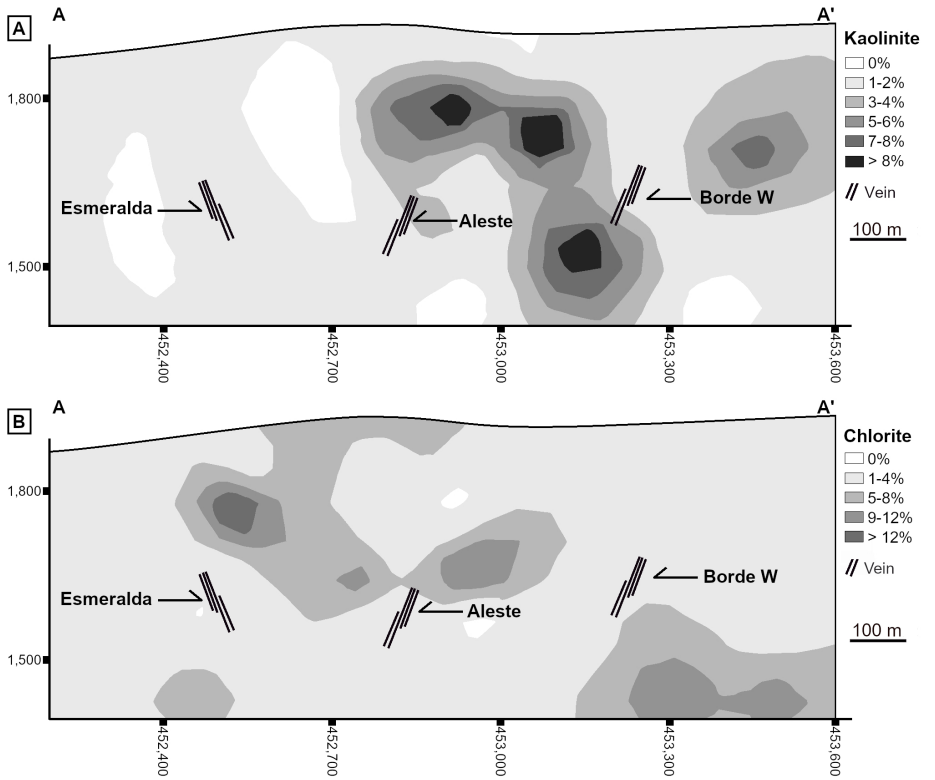

FIG. 8. Distribution of kaolinite (A) and chlorite (B) in the Aleste vein cross section.

5. Discussion

5.1. Mineral identification and semi-quantification by a XRD method

X-Ray diffraction proves to be useful in the recognition of minerals phases in hydrothermally altered rocks. In the case of adularia, the challenge is to identify this mineral in the diffractogram when it coexists with other K-bearing feldspars, mainly orthoclase and microcline. This study identified four secondary peaks in the diffractogram of the standard mineral, which can be useful to distinguish the presence of adularia in multimineral diffractograms of the studied samples. Despite, not further information of the Guanajuato adularia used as standard was provided by Yamana company, this specimen is from the Ag-Au epithermal veins of the Guanajuato mining district (Gross, 1975; Solé *et al*., 2021), which make this mineral suitable for this study. Even with this, it is known that the diffractograms of the same mineral can show differences in peaks distribution related to the ordering degree of the crystallographic structure and contents of trace elements (Colville and Ribbe, 1968; Stewart and Ribbe, 1969; Ferguson *et al*., 1991). Although the geological environments are similar between both the standard and the El Peñón adularias, could be some shift in the position of some peaks. So, we recommended for these types of studies, to obtain pure adularia samples from low sulfidation deposits located close to the prospection areas. Thus, would be ensured that the geological setting, the mineral geochemistry, and crystallographic structure would be closer to the mineral in search, and therefore, the standard diffractogram can be more precise, increasing the chance of success in the mineral prospection stage.

Adularia semi-quantification shows a very good correlation between the adularia content in a range between ~25 to 40% and the gold mineralized areas. Indicating that zones with this range of adularia abundance are favorable areas for gold prospection. However, the TOPAS software shows to be limited

when two K-feldspars are quantified in the same diffractogram, which could overestimate the adularia content in detriment to the abundance of orthoclase. This problem could be solved by the use of an updated software version that focuses its quantification by using the secondary peaks of the minerals. Even with this limitations, this mineralogical study shows to be useful for the prospection of low sulfidation gold deposits.

5.2. Identification of low abundance clay minerals

Regarding the low abundance of clays, as smectites, these minerals cannot be efficiently identified by X-Ray diffraction. This problem is due to the high percentages of other minerals present such as quartz and carbonates, and the range in which the diffractometer measures (2θ=3°-70°) that causes the concealment of low abundance clay peaks by the background noise. Thus, we propose the XRD oriented aggregates study (Poppe *et al*., 2001), which focuses on the detection of low percentages of minerals by intensifying their peaks in the diffractogram. This type of analysis facilitates the development of detailed studies of the behavior of low-abundance minerals in the alteration haloes in the epithermal environment to be used as a proxy for the prospection of low sulfidation veins.

5.3. Hydrothermal alteration haloes definition

Alteration halos commonly described in low sulfidation epithermal deposits (*e.g*., Hedenquist *et al*., 2000; Simmons *et al*., 2005; Camprubí and Albinson, 2006; Warren *et al*., 2007) are clearly identifiable in the results of the XRD mineralogical analyses presented in this work. The changes observed in the hydrothermally altered wall rocks moving away from the internal zones with adularia to sericite, illite, illite-smectite, and finally, to kaolinite, expressing the hydrothermal fluid evolution from a high temperature, and near neutral pH solution in the mineralized zone, to a low temperature, and slightly acid-solution at the boundaries of the system (Hedenquist *et al*., 2000).

5.3.1. Adularia-quartz-carbonates-gold association

This K-feldspar is commonly found associated with low sulfidation epithermal deposits, its crystallographic structure changes from a maximum microcline to disordered high sanidine (the latter used in this study) according to the physicochemical conditions at the time of formation (Ferguson *et al*., 1991). Usually, adularia precipitate in low-sulfidation veins as fine-grained euhedral rhombic crystals, sub-rhombic, tabular, and pseudo-acicular, accompanied by colloform to crustiform quartz, platy calcite, and ore minerals (Dong and Morrison, 1995; Simmons *et al*., 2005). This mineral is often associated with quartz and carbonates, this association is interpreted as the product of boiling of the hydrothermal fluid at around 1 to 2 km deep below the water table (Simmons *et al*., 2005). Thin section descriptions of samples of the El Peñón deposit agree with the descriptions made by Simmons *et al*. (2005), showing rhombic adularia crystals associated with quartz and carbonates (Fig. 9). Based on the study by Dong and Morrison (1995), the adularia shape suggests a prolonged boiling that produced a drop in temperature (<220 °C) which is faster than the loss of CO_2, triggering the dissolution of previously formed carbonates in the earliest steps of the boiling at high-CO_2 fugacity and the replacement of them by adularia and quartz. Additionally, in prolonged boiling, the loss of H_2S induces the precipitation of gold from bisulfide complexes $(Au(HS)_2^-$, according to the following equation (Dong and Morrison,1995):

$$8Au(HS)^{2-}(aq)+4H_2O(aq)+6H^+(aq)\rightarrow 8Au^0+15H_2S(aq)+SO_4^{2-}(aq) \quad (\mathbf{1})$$

These processes explain the association between gold and the quartz-adularia alteration in the mineralized zones in the El Peñón veins. In addition, the paragenesis of adularia, siderite, rhodochrosite, ankerite, calcite, quartz and sulfide observed in the XRD analyses confirm the observations by Bissig *et al*. (2007) who reported the relationship between these minerals and the gold mineralization in the El Peñón veins, based on descriptions and elemental analysis (ICP-AES) in carbonate minerals.

5.3.2. Sericite and illite

These minerals are the product of plagioclase and K-feldspar alteration by hydrothermal fluids with a slightly acidic pH, and temperatures between ~150 and 350 °C, in the epithermal environment (Hedenquist *et al*., 2000). Sericite is a term that refers to a fine-grained aggregate of white micas, as muscovite, that are commonly a product of feldspar

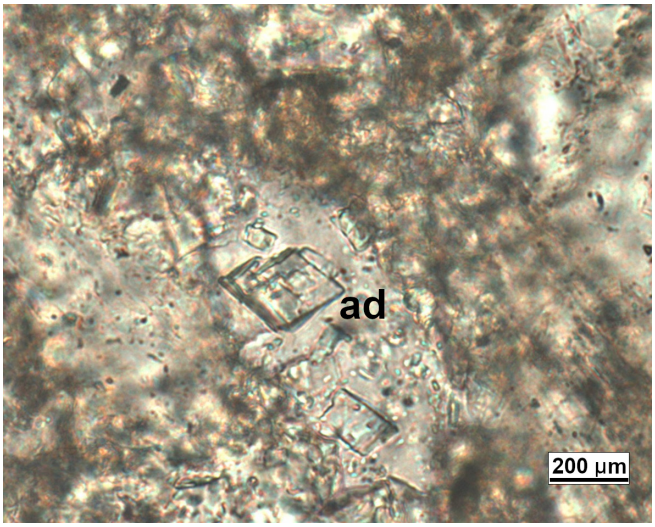

FIG. 9. Pseudo rhombic adularia crystals from quartz-carbonate-adularia alteration in the Aleste vein. **ad:** adularia.

alteration. In low-sulfidation epithermal environments, this mineral is the product of the feldspar alteration due to temperature- and pH-decrease of the post boiling activity of the hydrothermal fluid (Dong and Morrison, 1995). Instead, illite is a clay with similar geochemical composition to sericite, but with a smaller grain size and deficit of potassium in its structure. This fine-grained mica helps to interpret the temperature variation in the system; thus, it is useful as an indicator of the zones where the hydrothermal fluid passed, decreasing in temperature (under 300° C; Hedenquist *et al*., 2000).

The occurrence of sericite in XRD analyses of samples from veins in the El Peñón deposit was previously described only by Pérez (1999), other studies do not describe this mineral in the district, being illite the only K-bearing mineral in addition to adularia in the El Peñón veins (*e.g*., Cabello, 1999; Robbins, 2000; Zuluaga, 2004; Warren *et al*., 2004, 2007; Bissig *et al*., 2007; Donoso, 2012). Sericite detection in XRD analyses is associated with the appearance of Muscovite M1 pattern (Zadina, 1982) from the PDF-2 database in the diffractograms obtained. In the analyses, the presence of sericite and illite could be due to the potassium content in the crystal, variation in the structural order and variation in their granulometry, or just product of alteration of the first for the second mineral phase. Potassium-rich minerals, such as sericites, dominate in the areas closest to the ore, varying to clays with higher silica content towards the margins of the system, with clay minerals such as illite and illite-smectite (Rosenberg, 2002). Thus, in the El Peñón, the K-bearing minerals vary from sericite near the core to illite and finally, smectite at the boundary of the system, in accordance with the transition of K-metasomatism, pH and temperature changes in low-sulfidation epithermal environments (Hedenquist *et al*., 2000; Sillitoe and Hedenquist, 2003; Simmons *et al*., 2005; Warren *et al*., 2007). The distribution of these minerals can clearly be seen in figure 7. Indeed, the distribution and semi-quantitative abundance of potassic minerals reflex the evolution of the fluids from the vein and core of the epithermal system to the outer zones, represented by the precipitation of adularia in the mineralized zones changing to sericite, later to illite in the outer areas. Indicating that the fluids moved upward through the structures, with decreasing temperature and increasing acidity (*e.g*., pH 4 to 5) as it moves away from the mineralized zones (Fig. 10).

5.3.3. Kaolinite

This mineral is the product of the alteration of micas, plagioclase, and K-bearing minerals by hydrolysis reactions (Hemley and Jonas, 1964), being part of the argillic and advanced argillic alterations. In low sulfidation epithermal veins, this mineral is associated with steam-heated and supergene environments, the last one associated with

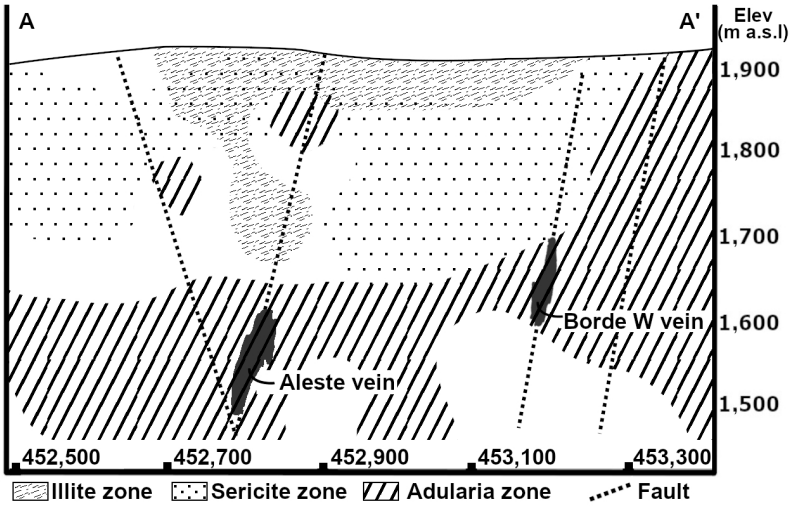

FIG. 10. Schematic distribution of K-bearing alteration minerals in the A-A' Aleste vein cross section, based on the semi-quantitative amount obtained by XRD for each mineral. Adularia content = >20%, sericite content = >10%, illite content = >7%. Some minor amounts of these minerals can overlap the other haloes. For more information about the semi-quantitative amount of each mineral see figures 6, 7 and 8.

oxidation of sulfide minerals after the hydrothermal event (Hedenquist *et al*., 2000; Simmons *et al*., 2005; Warren *et al*., 2007).

In the studied samples, it is possible to recognize two mineral associations that accompany kaolinite: **i**) the mineral assemblage of kaolinite, quartz, carbonates, montmorillonite, sericite and/or illite. This mineral association indicates a genesis related to steam-heated CO_2-rich fluids, coming from the boiling zone, with a pH ~4 to 5 in a low O_2-availability environment, which creates intermediate argillic haloes below the water table and in the margins of the hydrothermal system (Hedenquist and Arribas, 2021). Instead, **ii**) the mineral association of kaolinite with carbonates, gypsum, hematite, jarosite, alunite, heulandite and montmorillonite and minor amounts of relict pyrite reflects a post-hydrothermal supergene alteration at low temperature (~40 °C) and an oxidizing environment. This alteration overprinted the hydrothermal alterations above the water table.

5.3.4. Chlorite

This mineral represents the distal propylitic alteration zone of the epithermal system. It can also be observed in andesitic dikes with a high content of Na-, Mg- and Ca-bearing minerals that induce the formation of chlorite, calcite, and epidote as alteration minerals. Chlorite is abundant in low-sulfidation deposits to the detriment of epidote which is common at a deeper environment. The cross section shows that the propylitic alteration is far from quartz-adularia veins and represents the margins of the epithermal system.

6. Summary and Conclusion

This study confirms that the X-ray diffraction method is reliable for the determination of adularia in multi-mineral diffractograms, demonstrating that this technique can be useful for targeting new mineralized veins in low sulfidation epithermal deposits. The spatial distribution of the alteration minerals in the studied cross section at El Peñón define the typical alteration halos described in Au-Ag low sulfidation epithermal deposits. In the veins from El Peñón deposit the following statements can be made:

The method to identify adularia and other minerals by using XRD demonstrated its usefulness for the definition of new prospection targets at El Peñón.

Adularia occurs mainly 100 m below the surface with great extension and abundance in the rhyolitic rock unit (informally called Riolita Fluidal-Bandeada unit (FBR)) and restricted in intermediate composition rocks. This mineral is closely correlated with the Au ore zones in the Aleste, Esmeralda and Borde W veins, being adularia semi-quantitative

abundance between 25 to 40% a good indicator of gold mineralization.

Sericite and illite occur mainly above 100 m depth in areas where adularia is scarce or absent. The distribution of these K-bearing minerals together with adularia show the evolution of the hydrothermal fluid, and the structural control in the fluid flow, represented by a high content of adularia in the mineralized core changing to sericite, and illite to shallow areas, these minerals are always associated with a high content of quartz, carbonates, and lesser amounts of smectites, and pyrite.

Kaolinite is related to both argillic alterations caused by steam-heated fluids and to advanced argillic alteration associated with supergene alteration processes. Thus, the minerals associated with kaolinite are important in determining if the prospecting for low sulfidation epithermal veins is being conducted in the right environment.

Chlorite is indicative of propylitic alteration. This alteration usually is far from the mineralized areas, so this mineral is a reliable indicator of the margins of the hydrothermal system. This mineral can be useful in limiting the prospecting areas.

Acknowledgements

This work was financed by the Yamana Gold Company, El Peñón mine division. F. Álvarez is greatly acknowledged for his technical assistance with the X-ray diffraction analyses and lab work at Geochemical lab of the Universidad Católica del Norte. We are also grateful to the exploration division of El Peñón deposit for invaluable logistic support and for providing the samples for this study. Thanks to Dra. E. Fonseca, and Dr. W. Vivallo which provided reviews that greatly improved the manuscript.

References

Bissig, T.; Donoso, D.; Guerra, N.; Dipple, G. 2007. Vein carbonates in the low sulfidation epitermal Au-Ag District of El Peñón, II Región, Chile: Environment of formation and exploration implications. Revista Geológica de Chile 34 (2): 291-303.

Boric, R.; Díaz, F.; Maksaev V. 1990. Geología y yacimientos metalíferos de la Región de Antofagasta. Servicio Nacional de Geología y Minería, Boletín No. 40: 246 p. Santiago.

Cabello, P. 1999. Geología Distrital y Mineralización Aurífera Asociada a Domos Riolíticos en el Yacimiento El Peñón; II Región de Antofagasta. Memoria de Título (Inédito), Universidad de Chile, Departamento de Geología: 74 p.

Camprubí, A.; Albinson, T. 2006. Depósitos epitermales en México: actualización de su conocimiento y reclasificación empírica. Sociedad Geológica Mexicana, Boletín 58 (1): 27-81.

Camprubí, A.; González-Partida, E.; Levresse, G.; Tritlla, J.; Carrillo-Chávez, A. 2003. Depósitos epitermales de alta y baja sulfuración: una tabla comparativa. Sociedad Geológica Mexicana, Boletín 56 (1): 10-18.

Camus, F. 2003. Geología de los Sistemas Porfíricos en los Andes de Chile. Servicio Nacional de Geología y Minería: 267 p. Santiago.

Černý, P.; Chapman, R. 1984. Paragenesis, chemistry and structural state of adularia from granitic pegmatites. Bulletin de Minéralogie 107 (3-4): 369-384.

Colville, A.; Ribbe, P. 1968. The crystal structure of an adularia and a refinement of the structure of orthoclase. The American Mineralogist 53: 25-37.

Cornejo, P.; Matthews, S.; Pérez de Arce, C. 2003. The "K-T" compressive deformation event in northern Chile (24-27°S). *In* Congreso Geológico Chileno, No. 10, CD-Rom: 1-13. Concepción.

Dong, G.; Morrison, G.W. 1995. Adularia in epithermal veins, Queensland: morphology, structural state and origin. Mineralium Deposita 30 (1): 11-19.

Donoso, F.J. 2012. Caracterización petrográfica y mineralógica de la veta Bonanza Aleste y sus implicancias geometalúrgicas, mina El Peñón, región de Antofagasta. Memoria de título (Inédito), Universidad Católica del Norte: 73 p.

Einaudi, M.T.; Hedenquist, J.W.; Inan, E.E. 2003. Sulfidation state of fluids in active and extinct hydrothermal systems: Transitions from porphyry to epithermal environments. Society of Economic Geologists, Special Publication 10: 285-314.

Ferguson, R.; Ball. N.; Černý, P. 1991. Structure refinement of an adularian end-member high sanidine from the Buck Claim Pegmatite, Bernic Lake, Manitoba. Canadian Mineralogist 29: 543-552.

Giggenbach, W.F. 1988. Geothermal solute equilibria: Derivation of Na-K-Mg-Ca geoindicators. Geochimica et Cosmochimica Acta 52: 2749-2765.

Gross, W.H. 1975. New ore discovery and source of silver-gold veins, Guanajuato, Mexico. Economic Geology 70: 1175-1189.

Guilbert, J.; Park, C. 2007. The Geology of Ore Deposits. Waveland Press, Inc.: 985 p. Illinois.

Hedenquist, J.W.; Arribas, A.R. 2021. Exploration Implications of Multiple Formation Environments of

Advanced Argillic Minerals. Economic Geology: 35 p.

Hedenquist, J.W.; Arribas, A.R.; González-Urien, E. 2000. Exploration for epithermal gold deposits. Society of Economic Geologist, Reviews in Economic Geology 13: 245-277.

Hemley, J.J.; Jones, W.R. 1964. Chemical aspects of hydrothermal alteration with emphasis on hydrogen metasomatism. Economic Geology 59: 538-569.

Holley, E.A.; Bissig, T.; Monecke, T. 2016. The veladero high-sulfidation epithermal gold deposit, El Indio-Pascua Belt, Argentina: Geochronology of alunite and jarosite. Economic Geology 111 (2): 311-330.

Lenton, P.G. 1979. Mineralogy and Petrology of the Buck Claim Lithium Pegmatite, Bernic Lake, Southeastern Manitoba. M.Sc. Thesis (Unpublished), University of Manitoba: 180 p.

Marinovic, N.; Smoje, I.; Maksaev, V.; Hervé, M.; Mpodozis, C. 1995. Hoja Aguas Blancas, Región de Antofagasta. Servicio Nacional de Geología y Minería, Carta Geológica de Chile 70: 150 p., escala 1:250.000, Santiago.

Matthews, S. 2009. Geocronología de eventos hidrotermales en el Bloque Norte de El Peñón. Comparación con el Bloque Peñón y Eventos Magmáticos.Yamana Gold, Internal report: 14 p.

Pérez, M. 1999. Alteración hidrotermal en el depósito epitermal de Au-Ag El Peñon, II Región Antofagasta. Memoria de Título (Unpublished), Universidad de Chile, Departamento de Geología: 109 p.

Poppe, L.J.; Paskevich, V.F.; Hathaway, J.C.; Blackwood, D.S. 2001. A laboratory manual for X-ray powder diffraction. United States Geological Survey, Open-File Report 01-041: 88 p.

Robbins, C. 2000. Geology of the El Peñón gold-silver deposit, Northern Chile. *In* Geology and Ore Deposits 2000: The Great Basin and Beyond Symposium. Geology Society of Nevada Symposium Proceedings: 249-264.

Rosenberg, P.E. 2002. The nature, formation, and stability of end-member illite: A hypothesis. American Mineralogist 87: 103-107.

Sillitoe, R.H. 1993. Epithermal models: genetic types, geometrical controls and shallow features. *In* Mineral Deposit Modeling (Kirkham, R.V.; Sinclair, W.D.; Thorpe, R.I.; Duke, J.M.; editors). Geological Association of Canada, Special Paper 40: 403-417.

Sillitoe, R.H. 2015. Epithermal paleosurfaces. Mineralium Deposita 50 (7): 767-793.

Sillitoe, R.H.; Hedenquist, J.W. 2003. Linkages between volcanotectonic settings, ore-fluid compositions, and epithermal precious-metal deposits. Society of Economic Geologists, Special Publication 10: 315-343.

Simmons, S.F.; White, N.C.; John, D.A. 2005. Geological characteristics of epithermal precious and base metal deposits. Economic Geology 100th Anniversary: 485-522.

Simpson, M.; Mauk, J.L.; Simmons, S.F. 2001. Hydrothermal Alteration and Hydrologic Evolution of the Golden Cross Epithermal Au-Ag Deposit, New Zealand. Economic Geology 96 (4): 773-796.

Solé, J.; Pi-puig, T.; Ortega-Rivera, A. 2021. A Mineralogical, Geochemical, and Geochronological Study of "Valencianite" from La Valenciana Mine, Guanajuato, Mexico. Minerals 11 (7): 741. doi: 10.3390/min11070741.

Stewart, D.B.; Ribbe, P.H. 1969. Structural explanation for variations in cell parameters alkali feldspar with Al/Si ordering. American Journal of Science 267-A: 444-462.

Warren, I.; Zuluaga, J.I.; Robbins, C.H.; Wulftange, W.H.; Simmons, S.F. 2004. Geology and geochemistry of epithermal Au-Ag mineralization in the El Peñón Mine, Northern Chile. Society of Economic Geologists, Special Publication 11: 113-139.

Warren, I.; Simmons, S.F.; Mauk, J.L. 2007. Whole-rock geochemical techniques for evaluating hydrothermal alteration, mass changes, and compositional gradients associated with epithermal Au-Ag mineralization. Economic Geology 102 (5): 923-948.

Warren, I.; Archibald, D.A.; Simmons, S.F. 2008. Geochronology of epithermal au-ag mineralization, magmatic-hydrothermal alteration, and supergene weathering in the El Peñón district, northern Chile. Economic Geology 103 (4): 851-864.

Zadina, W. L. 1982. Structural variations of muscovite in porphyry copper systems. M.Sc. Thesis (Unpublished), University of Arizona: 81 p.

Zuluaga, J.I. 2004. Geología y Mineralización del Distrito El Peñón, Segunda Región de Antofagasta, Chile. Tesis de Magíster en Geología Económica (Inédito), Universidad Católica del Norte: 150 p.

Manuscript received: June 03, 2021; revised/accepted: November 02, 2021; available online: January 31, 2022.

Supplementary material 1

Basic instrumental parameters for the iterative method used for the semi-quantification of mineral contents, in whole rock samples, used in the XRD/XRF laboratory, at Universidad Católica del Norte.

Background	Use	Value	Code
Chebychev	yes	-	@
Order	-	7	-
	-	-	-
1/X Bkg	no	1,000	Refine
Goniometer Radii	-	-	-
Primary Radius (mm)	-	217.5	-
Secondary Radius (mm)	-	217.5	-
Equatorial Convolutions	-	-	-
RS Width (mm)	yes	0.2	Fix
FDS Angle (°)	yes	1	Fix
VDS Length (mm)	no	12	Fix
VDS Scale Intensity	no	-	-
Tube Tails	yes	-	-
Source Width (mm)	-	0.04	Refine
Z1 (mm)	-	-1	Refine
Z2 (mm)	-	1	Refine
Fraction	-	0.005	Refine
Axial Convolutions	-	-	-
Simple Axial Model (mm)	no	12	Fix
Full Axial Model	yes	-	-
Source Length (mm)	-	12	Refine
Sample Length (mm)	-	20	Refine
RS Length (mm)	-	12	Refine
Prim. Soller (°)	yes	2.3	Refine
Sec. Soller (°)	yes	2.3	Refine
Peak shift	-	-	-
Zero error	no	0	Refine
Sample disp. (mm)	yes	0	Refine
Intensity Correction	-	-	-
LP factor	yes	26.64	Fix
Sample Convolutions	-	-	-
Absorption (1/cm)	no	100	Refine
Sample Tilt (mm)	no	0	Refine
Miscellaneous	-	-	-
Conv. Steps	-	1	-
Start X	no	0	-
Finish X	no	0	-
Fixed WL Neutron	no	-	-
Hats Conv.	no	0.1	Fix

Supplementary material 2

The mineral content determinations was achieving following three semi-quantifications:

A) Semi-quantification considering orthoclase as a representative of K-feldspar groups (excluding adularia).

B) Semi-quantification considering adularia as a representative of K-feldspar groups (excluding orthoclase).

C) Semi-quantification considering both orthoclase and adularia.

The use of these three iterations is to determine if the TOPAS software is able to semi-quantify the content of adularia and orthoclase in the same sample, obtaining a percentage not far from the total abundance of K-feldspar.

Below is an example of these three semi-quantification in one of the diffractogram of a sample analyzed by XRD (Table S2; Fig. S1). It shows the results of each quantifications, the similarities in the iterations indicate that both minerals are in the sample and the semi-quantification is good, thus iteration c) is able to be used.

TABLE S2. SEMI-QUANTIFICATIONS REALIZED IN SAMPLE SPA-0011-229 IN BASE OF THE METHODOLOGY PROPOSED.

Sample: SPA-0011-229	A	B	C
Quartz	17	16	16
Orthoclase	56	-	23
Adularia	-	56	36
Albite	16	15	14
Sericite	5	5	5
Ankerite	6	6	6
Chlorite	T	T	T
Pyrite	T	T	T
Gypsum	T	T	T
Σ Feldespatos-K	**56**	**58**	**59**

The amount of total K-feldspar in each iteration are similar, thus the presence, and quantification of these three minerals can be confirmed.

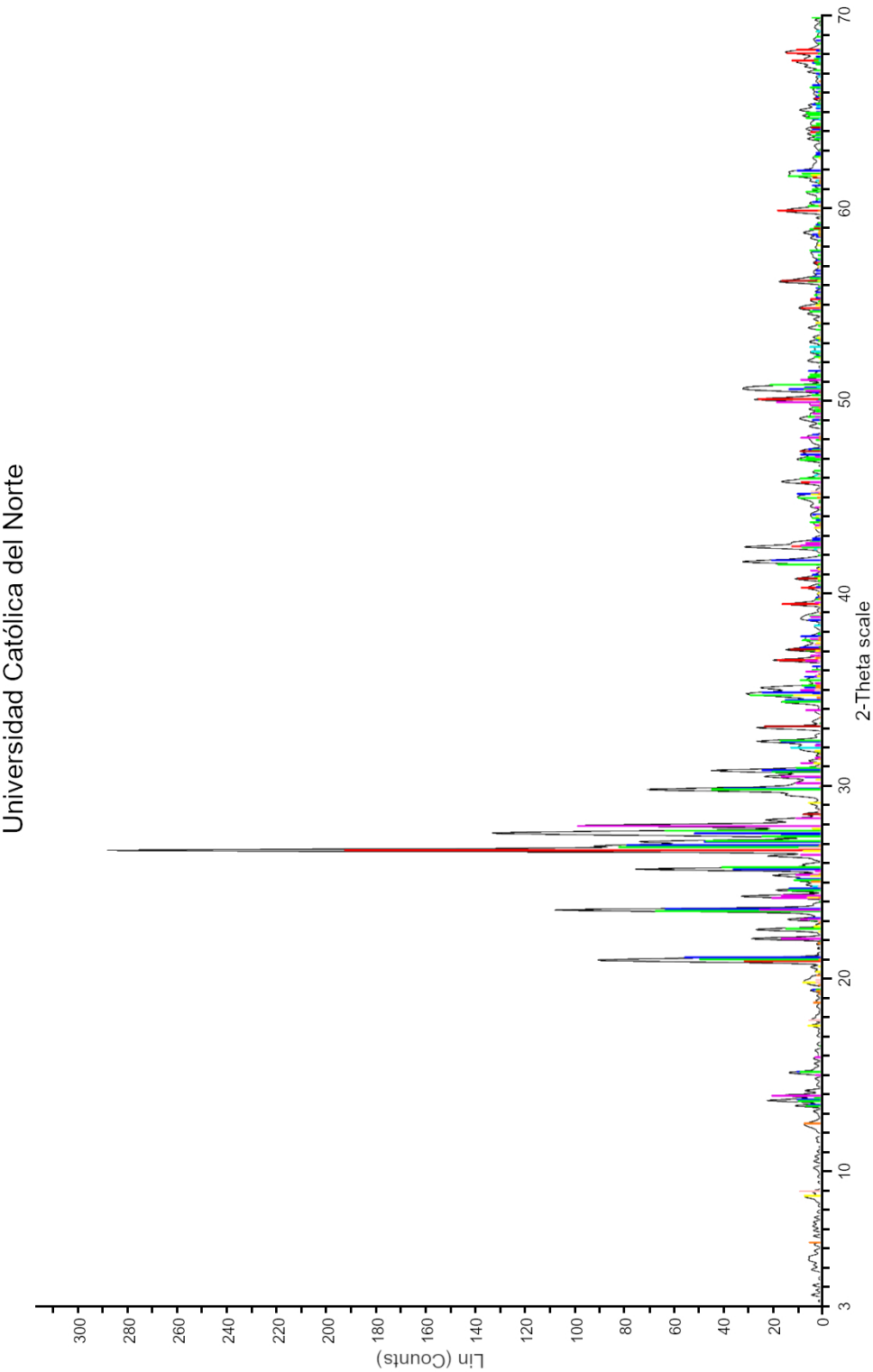

FIG. S1. Diffractogram of sample SPA-0011-229 with all the mineral phases detected.

Supplementary material 3

TABLE S3. X-RAY DIFFRACTION ANALYSES AND SEMIQUANTIFICATION OF THE PHASES PRESENT IN EACH SAMPLE. THE 100% CORRESPOND TO THE TOTAL OF CRYSTALLINE PHASES NOT COUNTING TRACE MINERALS (<2% OF ABUNDANCE) AND THE AMORPHOUS PORTION OF THE ROCK.

Drilling: SEE-0011

Sample	Quartz	Albite	Orthoclase	Adularia	Sericite	Calcite	Ankerite	Chlorite	Pyrite	Jarosite	Gypsum	Magnetite
SEE-0011-034	45	26	-	26	-	-	-	-	-	-	-	2
SEE-0011-061	28	36	30	-	-	3	-	-	T	2	-	T
SEE-0011-089	40	25	16	-	16	-	-	-	-	2	-	-
SEE-0011-107	36	7	5	35	11	-	-	3	T	3	-	-
SEE-0011-113	31	4	22	43	-	-	T	-	T	-	-	-
SEE-0011-117	46	5	16	33	-	-	-	-	T	-	-	-
SEE-0011-121	21	3	14	62	-	-	-	-	-	-	-	-
SEE-0011-127	41	8	26	25	-	-	-	-	T	-	-	T
SEE-0011-137	37	7	24	31	T	-	-	-	T	-	-	T
SEE-0011-187	38	11	3	35	10	-	-	2	-	T	T	-
SEE-0011-237	40	22	31	-	6	T	T	-	-	-	-	-
SEE-0011-287	52	15	15	-	14	4	-	-	-	-	-	-
SEE-0011-310	25	42	19	-	6	4	-	4	-	-	-	-

Drilling: SNX-0125

Sample	Quartz	Albite	Orthoclase	Adularia	Sericite	Kaolinite	Calcite	Ankerite	Chlorite	Pyrite	Hematite	Smectite	Gypsum	Anhydrite	Analcime
SNX0125-008	16	45	16	T	3	-	2	-	5	-	5	T	-	6	2
SNX0125-033	39	27	8	-	23	-	T	-	2	-	-	-	T	-	-
SNX0125-058	42	21	25	-	12	-	T	-	T	-	-	-	T	-	-
SNX0125-091	17	25	T	-	25	-	9	-	24	-	-	-	-	-	-
SNX0125-133	18	20	6	-	26	-	4	11	15	-	-	-	-	-	-
SNX0125-176	40	24	36	-	T	T	-	-	-	T	-	-	-	-	-
SNX0125-186	44	12	38	-	6	-	T	-	-	T	-	-	-	-	-
SNX0125-192	26		69	-	2	2	T	-	-	T	-	-	-	-	-
SNX0125-196	45	4	43	-	-	4	4	-	-	T	-	-	-	-	-
SNX0125-200	46	12	42	-	-	T	T	-	-	T	-	-	-	-	-
SNX0125-206	43	12	45	-	-	T	T	-	-	-	-	-	-	-	-
SNX0125-216	41	8	48	-	-	2	-	-	-	-	-	-	-	-	-
SNX0125-266	26	19	5	46	-	-	-	2	-	T	-	2	-	-	-
SNX0125-306	26	13	14	38	-	7	T	-	-	T	-	2	T	-	-
SNX0125-315	26	3	3	55	8	2	-	3	-	-	-	-	-	-	-

Drilling: SAI-0104

Sample	Quartz	Albite	Orthoclase	Adularia	Sericite	Illite	Kaolinite	Calcite	Ankerite	Siderite	Chlorite	Pyrite	Hematite	Magnetite	Smectite	Gypsum	Pentahydrite	Hornblende	Epidote
SAI-0104-018	15	48	T	18	T	T	T	3	-	-	6	T	5	-	-	-	4	-	-
SAI-0104-043	34	28	6	-	21	T	-	5	-	-	6	T	T	-	-	T	-	-	-
SAI-0104-068	39	26	T	23	T	3	-	-	4	-	2	T	T	-	3	-	-	-	-
SAI-0104-093	31	17	2	33	7	2	-	-	4	-	3	-	-	-	-	-	-	-	-
SAI-0104118	21	34	2	16	8	4	-	3	6	-	4	T	-	-	2	T	-	-	-
SAI-0104-143	5	24	20	5	6	T	-	9	-	-	21	-	-	2	-	-	-	T	7
SAI-0104-168	30	12	T	43	8	-	-	-	2	T	T	T	-	T	-	T	-	4	-
SAI-0104-195	40	9	5	42	3	-	-	T	T	T	-	T	-	T	-	-	-	-	-
SAI-0104-205	37	20	5	28	5	-	-	2	2	T	T	T	-	T	-	T	-	-	-
SAI-0104-262	34	13	6	43	4	-	-	-	-	T	-	T	-	-	-	-	-	-	-
SAI-0104-215	29	8	10	49	3	-	-	T	-	-	T	-	-	-	-	-	-	-	-
SAI-0104-219	37	33	3	26	T	-	-	-	-	T	-	-	-	-	-	-	-	-	-
SAI-0104-225	26	19	16	36	2	-	T	T	-	-	-	T	-	-	-	-	-	-	-
SAI-0104-235	27	19	8	44	-	-	-	T	-	-	2	T	-	-	-	-	-	-	-
SAI-0104-260	40	3	8	47	-	-	-	-	-	-	2	-	-	-	-	-	-	-	-

Drilling: SPA-0011

Sample	Quartz	Albite	Orthoclase	Adularia	Sericite	Illite	Kaolinite	Calcite	Ankerite	Siderite	Rhodochrosite	Chlorite	Pyrite	Hematite	Jarosite	Smectite	Gypsum	Halite	Heulandite	Alunite
SPA-0011-009	15	44	18	4	-	-	-	3	T	-	-	9	T	5	-	-	T	-	2	-
SPA-0011-018	17	42	T	13	-	10	-	6	-	-	-	7	T	4	-	-	-	-	-	T
SPA-0011-027	13	41	11	14	-	4	-	3	-	-	-	10	-	4	-	-	T	-	-	-
SPA-0011-036	13	51	16	-	2	11	-	3	-	-	-	-	T	4	-	-	T	-	-	-
SPA-0011-045	27	31	5	-	19	9	-	5	-	-	-	-	-	3	T	T	2	-	-	-
SPA-0011-054	34	29	5	-	31	-	-	T	T	-	-	-	T	-	T	-	-	-	-	-
SPA-0011-063	35	24	16	-	24	-	-	T	-	-	-	-	-	-	-	-	T	-	-	T
SPA-0011-072	23	23	1	26	11	-	6		5	-	-	-	-	T	-	2	2	-	-	-
SPA-0011-081	34	15	3	27	-	-	4	T	4	-	-	2	T	-	-	10	T	-	-	-
SPA-0011-090	33	23	12	14	-	-	8	T	3	-	-	3	T	-	-	4	T	-	-	-
SPA-0011-099	26	19	3	30	-	-	8	2	4	-	-	5	T	-	-	3	-	-	-	-
SPA-0011-108	33	12	2	33	-	-	11	3	-	-	-	4	T	-	T	2	T	-	-	-
SPA-0011-117	27	16	3	37	8	-	4	T	-	-	-	4	T	-	-	-	T	-	-	-
SPA-0011-126	23	29	6	6	22	-	4	2	3	-	-	-	-	-	-	2	2	-	-	-
SPA-0011-135	22	37	16	-	14	-	4	2	5	-	-	-	-	-	-	-	T	-	-	-
SPA-0011-149	5	29	14	12	-	-	-	8	T	-	-	28	-	4	-	-	T	-	T	-
SPA-0011-251	11	32	3	44	T	-	-	2	-	2	-	6	T	-	-	-	T	-	-	-
SPA-0011-189	40	3	13	39	-	-	4	-	T	-	-	-	-	-	-	-	-	T	-	-
SPA-0011-209	31	3	29	34	-	-	-	-	2	T	-	-	T	-	-	-	-	-	-	-
SPA-0011-219	46	4	49	-	-	-	-	-	T	T	-	-	-	-	-	-	-	-	-	-
SPA-0011-221	40	6	53	-	-	-	T	-	T	T	-	-	T	-	-	-	-	-	-	-
SPA-0011-223	20	7	14	52	-	-	2	-	4	T	-	-	T	-	-	-	-	-	-	-
SPA-0011-225	20	15	12	41	6	-	-	-	T	2	-	3	T	-	-	-	-	-	-	-
SPA-0011-227	13	16	3	54	5	5	-	-	T	2	-	T	2	-	-	-	-	-	-	-
SPA-0011-229	15	14	23	36	5	-	-	-	6	-	-	T	T	-	T	-	T	-	-	-
SPA-0011-231	24	10	2	38	-	-	3	7	10	-	3	-	2	-	-	-	T	T	-	-
SPA-0011-232	25	6	9	59	-	-	-	T	-	T	-	T	T	-	T	-	-	-	-	-
SPA-0011-233	36	6	9	47	-	-	-	2	-	-	-	-	T	-	-	-	-	-	-	-
SPA-0011-235	42	6	11	39	-	-	-	2	-	-	-	-	T	-	-	-	T	-	-	-
SPA-0011-237	44	4	17	30	3	-	-	2	-	-	-	-	T	-	-	-	-	T	-	-
SPA-0011-239	34	10	4	44	2	-	-	3	-	-	-	2	T	-	T	-	-	-	-	-
SPA-0011-241	19	12	18	46	-	2	-	-	T	T	-	2	T	-	-	-	-	-	-	-
SPA-0011-243	8	10	7	48	6	-	20	-	-	T	-	-	T	-	-	T	T	-	-	-
SPA-0011-245	26	20	2	18	28	-	-	T	T	-	-	5	-	-	-	-	T	-	-	-

Drilling: SNX-0307

Sample	Quartz	Albite	Orthoclase	Adularia	Sericite	Illite	Kaolinite	Calcite	Ankerite	Siderite	Rhodochrosite	Chlorite	Pyrite	Hematite	Jarosite	Gypsum	Biotite	Heulandite	Magnetite
SNX-0307-015C	17	47	15	-	-	-	3	6	-	-	T	11	T	-	-	-	-	-	-
SNX-0307-039C	39	29	2	-	19	-	-	8	-	-	-	-	T	3	-	-	-	-	-
SNX-0307-063C	39	28	13	-	16	-	-	T	-	T	-	3	T	-	-	T	-	-	-
SNX-0307-090C	36	22	10	16	-	6	4	T	3	-	-	-	T	-	2	-	T	-	-
SNX-0307-114C	32	22	20	9	-	-	8	T	T	-	-	8	T	-	T	-	-	-	-
SNX-0307-138C	25	28	12	T	-	13	7	3	7	-	-	-	T	2	3	-	-	-	-
SNX-0307-165	38	11	36	T	8	-	T	-	-	T	-	6	T	-	T	-	-	-	T
SNX-0307-175	17	29	17	23	-	-	-	T	-	T	-	11	2	-	-	-	-	-	T
SNX-0307-181	41	12	38	-	2	-	T	4	-	T	-	3	T	-	-	-	-	-	-
SNX-0307-185	36	T	13	41	-	T	T	3	6	-	-	T	T	-	-	-	-	T	-
SNX-0307-189	42	12	12	31	2	-	-	-	T	-	-	T	T	-	-	-	-	-	T
SNX-0307-195	40	12	6	36	2	-	-	3	-	T	-	T	T	-	-	-	-	-	T
SNX-0307-205	33	T	26	34	2	-	T	-	-	T	-	4	-	-	-	-	-	-	-
SNX-0307-255	34	10	2	47	-	-	6	T	-	T	-	-	T	-	T	-	-	-	-
SNX-0307-305	26	22	17	21	-	7	T	2	-	-	-	-	-	T	4	-	-	-	-
SNX-0307-320	32	36	24	-	5	-	-	2	-	-	-	-	T	T	-	-	-	-	-

Drilling: SNX-0121

Sample	Quartz	Albite	Orthoclase	Adularia	Sericite	Illite	Kaolinite	Calcite	Ankerite	Siderite	Chlorite	Hematite	Natrojarosite	Smectite	Gypsum	Natrolite	Baryte	Anhydrite	Alunite
SNX-0121-005	17	39	11	-	10	7	-	5	-	-	6	3	-	-	T	-	-	2	-
SNX-0121-030	11	27	3	8	37	-	-	7	-	-	6	T	-	-	-	-	-	-	-
SNX-0121-055	32	-	17	43	-	-	8	-	-	-	-	-	-	-	-	T	-	-	T
SNX-0121-059	58	-	37	T	-	-	4	-	-	-	-	-	-	-	T	-	T	-	-
SNX-0121-063	30	-	23	35	3	-	9	-	-	-	-	T	-	-	-	-	-	-	-
SNX-0121-090	38	13	27	6	-	-	11	2	3	-	-	T	-	-	-	-	-	-	-
SNX-0121-115	28	32	11	T	28	-	-	T	-	-	-	T	-	-	-	-	-	-	-
SNX-0121-140	11	42	5	T	-	-	-	10	-	-	27	5	-	-	-	-	-	-	-
SNX-0121-165	40	4	11	24	17	-	-	2	-	-	2	-	T	-	-	-	-	-	-
SNX-0121-190	54	4	8	32	-	-	-	2	-	-	-	-	-	-	-	-	-	-	-
SNX-0121-215	38	10	24	28	-	-	-	T	-	T	-	-	-	-	-	-	-	-	-
SNX-0121-220	39	24	3	33	-	-	-	-	-	T	T	-	-	-	-	-	-	-	-
SNX-0121-223	34	22	4	36	-	-	-	-	-	T	3	-	-	-	-	-	-	-	-
SNX-0121-225	43	13	5	28	-	-	10	-	T	-	T	-	-	-	-	-	-	-	-
SNX-0121-227	21	34	4	21	-	-	-	4	T	-	13	2	-	-	-	-	-	-	-
SNX-0121-230	19	36	3	26	-	-	-	4	T	-	6	3	-	3	-	-	-	-	-
SNX-0121-235	23	26	4	27	12	-	-	3	-	-	4	T	-	-	-	-	-	-	-
SNX-0121-250	43	3	4	31	18	-	-	T	-	-	T	T	-	-	-	-	-	-	-

Drilling: SNX-0122

Sample	Quartz	Albite	Orthoclase	Adularia	Sericite	Illite	Kaolinite	Calcite	Ankerite	Chlorite	Hematite	Smectite	Gypsum	Anhydrite
SNX-0122-006	26	26	-	T	-	21	-	11	-	T	3	-	-	13
SNX-0122-031	29	21	-	16	27	-	-	3	2	-	2	-	-	-
SNX-0122-056	48	8	22	-	17	-	-	T	2	2	-	-	T	-
SNX-0122-081	42	5	30	-	-	-	11	6	-	6	-	-	-	-
SNX-0122-106	4	41	4	24	-	-	18	4	2	3	-	-	-	-
SNX-0122-131	26	9	12	-	34	-	2	4	7	6	-	-	-	-
SNX-0122-156	46	3	T	38	-	-	7	2	T	-	-	4	T	-
SNX-0122-166	31	T	28	32	-	-	8	T	-	-	-	-	T	-
SNX-0122-171	44	-	47	-	6	-	2	T	T	-	-	-	T	-
SNX-0122-174	40	9	43	-	-	-	7	T	-	-	-	-	T	-
SNX-0122-176	36	-	7	34	19	-	3	T	-	-	-	-	T	-
SNX-0122-178	32	2	T	29	32	-	T	T	-	-	-	4	T	-
SNX-0122-181	29	5	2	31	27	-	3	3	-	-	-	-	-	-
SNX-0122-186	55	-	27	-	-	-	14	3	-	-	-	-	T	-

Drilling: SNX-0361

Sample	Quartz	Albite	Orthoclase	Adularia	Sericite	Illite	Kaolinite	Calcite	Ankerite	Siderite	Rhodochrosite	Chlorite	Pyrite	Pirrhotite	Hematite	Natrojarosite	Jarosite	Magnetite	Baryte	Halite	Heulandite	Cristobalite
SNX-0361-012C	32	36	7	-	-	12	T	5	4	-	-	-	-	-	3	T	-	-	-	-	-	-
SNX-0361-036C	42	25	5	-	23	-	-	4	-	-	-	-	-	-	T	T	-	-	-	-	-	-
SNX-0361-060C	41	23	2	8	20	-	T	3	2	-	-	-	-	-	-	T	-	-	-	-	-	-
SNX-0361-084C	42	14	12	11	16	-	3	2	-	-	-	-	-	-	-	-	-	-	-	-	T	-
SNX-0361-111C	31	7	T	4	37	-	T	6	4	-	-	4	-	-	T	-	6	-	-	-	-	-
SNX-0361-135C	40	-	11	46	-	-	T	2	-	T	-	-	T	-	T	-	-	-	T	-	-	-
SNX-0361-139C	38	-	30	30	-	-	T	-	-	-	-	-	-	-	-	-	2	-	T	-	-	-
SNX-0361-144C	37	-	30	22	8	-	-	-	-	-	-	-	T	-	T	-	2	-	T	-	-	-
SNX-0361-148	32	-	25	38	-	-	-	-	-	T	T	-	T	-	-	-	3	-	2	-	-	-
SNX-0361-152	36	-	26	35	-	-	-	-	T	-	-	-	-	T	-	-	-	-	2	-	-	-
SNX-0361-158	28	2	29	37	-	-	-	2	-	-	-	2	-	-	-	-	-	-	-	T	-	-
SNX-0361-168	33	-	15	48	-	-	-	-	T	-	-	3	T	-	-	-	-	-	-	-	-	-
SNX-0361-218	34	-	26	31	-	-	-	T	2	T	-	6	-	-	-	-	-	-	T	-	-	-
SNX-0361-268	39	-	17	21	10	-	7	5	T	T	-	T	-	-	-	-	-	-	T	-	-	-
SNX-0361-318	19	44	3	12	-	-	T	3	-	-	-	12	-	T	-	-	-	5	-	-	-	2
SNX-0361-368	26	35	5	9	11	-	-	2	-	-	-	12	-	-	-	-	-	-	-	-	-	-

Drilling: SNX-0123

Sample	Quartz	Albite	Orthoclase	Adularia	Sericite	kaolinite	Calcite	Ankerite	Chlorite	Pyrite	Hematite	Gypsum	Cristobalite	Halite	Anhydrite
SNX-0123-004	28	12	22	-	27	2	3	-	-	-	T	-	T	T	5
SNX-0123-028	48	-	5	45	T	-	-	-	2	-	-	-	-	-	-
SNX-0123-053	32	-	24	42	T	-	-	-	2	-	-	-	-	-	-
SNX-0123-078	38	-	9	49	-	4	-	-	-	-	-	-	-	-	-
SNX-0123-103	28	-	28	42	-	2	-	-	-	-	-	-	-	-	-
SNX-0123-128	30	6	4	44	-	11	4	-	-	-	T	T	-	-	-
SNX-0123-153	39	T	9	24	22	5	T	-	-	-	-	-	-	-	-
SNX-0123-178	23	-	25	50	-	-	-	T	2	-	-	T	-	-	-
SNX-0123-192	21	-	5	70	-	3	-	T	-	-	-	T	-	-	-
SNX-0123-258	21	T	6	69	3	-	T	-	T	-	T	-	-	-	T
SNX-0123-307	15	41	2	23	7	-	2	-	10	T	-	-	-	-	-

T: presence in traces (not quantifiable).